Trends in Biomaterials and Artificial Organs
sbaoi
www.biomaterials.org.in/tibao

Original Article

Polysaccharide-PVA/PEG blended Crosslinked Hybrid Hydrogels for Cardiac Tissue Engineering

Soumya K. Chandrasekhar[1,2], Joshi C. Ouseph[2*]

[1]*Department of Zoology, KKTM Government College (University of Calicut), Pullut, Kodungallur, Thrissur 680663, India*

[2]*Deptartment of Zoology, Christ College (University of Calicut), Irinjalakuda, Thrissur 680125, India*

Received: *9 October 2022*
Accepted: *7 January 2023*
Published online: *30 June 2023*

Keywords: *cardiac tissue engineering, hybrid hydrogels, biocompatibility, regenerative cardiology, polymeric blend*

As the native ECM exists as hydrogel, biocompatible polymeric hydrogel-based templates promise tissue engineering applications owing to their biomimetic nature. Hence, the choice of co-polymers employed is crucial in determining the cardiac performance of such hydrogels. On this juncture, the present study aimed to engineer biocompatible hybrid hydrogel scaffolds by the interpenetration and crosslinking of the natural polymers with synthetic polymers for cardiac regeneration. Two sets of hydrogels ACPVs (alginate, carboxy methyl cellulose and PVA as components) and ASPGs (Alginate, starch, and PEG as components) were prepared. FT-IR revealed the ample hydrophilic surface functional groups, water dynamics unveiled appreciable water holding capacity befitting native cardiac ECM, SEM analysis displayed surface porosity and dynamic contact angle unveiled the amphiphilic chemistry. The hydrogels were biodegradable as evaluated by aging in simulated biological fluids and the cytocompatibility was assessed with MTT cell viability assay and direct contact assay using H9c2 cardiomyoblasts. The hydrogel supported the growth and survival of H9c2 cardiomyoblasts onto the interstices. Also, the hydrogels were effective in imbibing antibiotics and arrested the growth of major Gram-positive and Gram-negative bacteria. Overall, the findings demonstrated that the reinforced hydrogel system exhibits optimum physicochemical properties, excellent biocompatibility, and appreciable biological performance to support cardiac cell growth suggesting the promising translational avenues in regenerative cardiology.

Introduction

World Health Organization (WHO) recently reported that cardiovascular diseases (CVDs) accounts ~17.9 million deaths globally [1]. Also, American Heart Association (AHA) estimated a 21.1% increase in global CVD deaths from 2007 to 2017 [2]. Among CVDs, the incidence of myocardial infarction (MI) is alarming as four out of every five CVD death is due to heart failure [3]. The ischemic damage following the MI impairs cardiac function and output. The conventional treatment strategies for managing MI rely on pharmacotherapy and surgical restitution; however, heart transplantation remains to be the ultimate management option. Moreover, necessity for lifelong medicines, dearth of organ donors, infection, and immunological rejections associated with transplantation surgery offer hurdles. Even though advancements in the field of biomedical engineering have been a boon in creating artificial organs, translational applications are limited warranting biocompatibility and functionality [4].

Cardiac tissue engineering (CTE) has been considered to be promising for the effective management of MI [5]. CTE approach triggers the inherent regenerative ability of human body by providing a supporting matrix loaded with specific cell phenotypes and growth factors using appropriate templates. The initial tissue consortium formed on such scaffolds accelerates ECM deposition restoring/regenerating the lost functions [6]. Importantly, meticulous designing of 3D scaffolds is important as the success rate depends solely on the performance of cells in scaffold until a functional cardiac extra cellular matrix (ECM) is being reconstructed by the surviving tissue. Hence, an ideal scaffold for CTE requires the physiochemical and biological properties identical to native cardiac ECM for supporting the formation of functional cardiac tissue [1]. In addition, the chance of infection warrants further

* *Coresponding author*
E-mail address: *sowmyakc.kc@gmail.com* (Dr. Joshi C. Ouseph Ph.D)

attention suggesting the scaffolds with antimicrobial properties [7].

On this background, the present study focused on the design and evaluation of a panel of hybrid hydrogel templates synthesized by interpenetrating the natural polysaccharide alginate, starch and the polysaccharide derivative carboxymethyl cellulose (CMC) with synthetic polymers such as poly(vinyl alcohol) (PVA) and poly(ethylene glycol) (PEG) for functional CTE applications.

Materials and Methods

Synthesis of hybrid hydrogels

Alginate-CMC-PVA (ACPV) hydrogels were prepared interpenetrating alginate, CMC and PVA. Briefly, 3% alginate was suspended in 5% Na_2HPO_4 which was mixed with 2% CMC and 5% PVA, followed by stirring the 1.5 % $CaCl_2$ and the mix was casted at 70°C overnight. The dried hydrogels were carefully removed from the petri dish and incubated in 10% $CaCl_2$ for an hour for additional crosslinking. Two batches of ACPV hydrogels, ACPV1 and ACPV2 were prepared which differs in alginate content: 5 ml and 10 ml respectively. The volume of PVA and CMC remained 5 ml each for both the batches. Similarly, the Alginate-starch-PEG (ASPG) hydrogels were prepared by mixing 3% alginate with 2% PEG in 5% starch blend following the above procedure. ASPG1 used 2.5 ml alginate and 5 ml blend whereas ASPG2 used 10 ml alginate and 5 ml blend. The hydrogel sheets were washed overnight in distilled water, freeze dried and stored at room temperature (RT) for further studies.

Analysis for surface functional groups

ATR spectrum, for assessing the surface functional groups, of ACPV and ASPG hybrid hydrogel subsets were recorded by using Nicolet iS50 FTIR spectrometer using lyophilized samples. Digitization and processing of the data were done using Microsoft Excel and Origin software was used to plot the spectra.

Equilibrium water content and weight swelling ratio

Freeze dried hydrogel samples were used to determine the water content and swelling capacity by soaking in distilled water (DW) and allowed to attain equilibrium for 24 h at RT. The swollen samples were wiped carefully using blotting paper to remove the excess water prior to weighing. The equilibrium water content and the swelling efficiency of the hydrogels were determined from the dry and wet weights following previously published reports [8].

Surface morphometry

The surface morphology and pore size of the scaffolds were determined using scanning electron microscope equipped with energy dispersive X-ray spectroscope (SEMEDAX). The average length and breadth of pores on scaffold surfaces were calculated from SEM images using ImageJ software using multi-measure plugin following previously published protocols [9].

Tensile strength

Tensile strength of water swollen hydrogels were determined using Shimadzu Universal Testing Machine (model AG-I) using dumb bell-shaped specimens (ISO 527-2 type 5A). Tensile strength was tested with a load cell of 100 N at RT with a crosshead speed of 10 mm/min. The tensile properties were determined as reported elsewhere [10].

Dynamic water contact angle

Six clean samples of uniformly rectangular shape and known width were swelled in distilled water and were used for determining the surface hydrophilicity by dynamic contact angle. The advancing and receding contact angle were determined by Wilhelmy method using KSV sigma 701 tensiometer by using distilled water as a solvent. The samples were immersed to a depth of 10 mm at a speed of 5 mm/min ignoring the first 2 mm length. The advancing and receding contact angle values were obtained automatically using the software associated with the instrument [9].

Biostability

The biostability of hybrid hydrogel subsets were determined by aging in PBS at RT. Changes in dry weight, pH, and total dissolved solids (TDS) were determined at a regular interval of 10 days for a period of 30 days [10].

Protein adsorption

The water swollen hydrogels were incubated with commercially available foetal bovine serum (FBS) (1:10 dilution in PBS) at 37°C on a shaker incubator overnight. Then the scaffolds were gently washed with PBS to remove the loose/unbound proteins, and vortexed in minimum PBS to extract the adhered proteins which were quantified by standard BCA method. Then percentage of proteins adsorbed on to the hydrogels was quantified with respect to total plasma protein content as control. SDS-PAGE using the extracted proteins was performed for assessing the extent of albumin adsorption using albumin (50μg/μl) as standard. The relative adsorption of albumin was calculated using the image analysis ImageJ software from the bands obtained the SDS-PAGE gels.

Cytocompatibility

Cell culture and maintenance

Rat cardiomyoblast cells (ATCC) was used for the cytocompatibility evaluations. The cells were grown in high glucose DMEM with 10% fetal bovine serum (FBS) (Cat# 30-2020, ATCC) at standard culture conditions (5% CO_2, 37°C, and antibiotics). Upon 70-80% confluence the cells were split using standard trypizinization protocols.

Cytotoxicity

The cytotoxicity of hydrogels extract (in cell culture medium) was determined by standard MTT assay using H9c2 cardiomyoblasts cell culture following previously reported protocol [11].

Direct contact assay

The toxicity of the hydrogels under the direct influence of cell contact was determined by direct contact assay. Then the hydrogel samples (10 mm diameter) were placed over the monolayer of H9c2 cells and allowed to proliferate for 24 h which were examined microscopically for alterations in morphology compared to the control.

Anti-microbial assay

The antibiotic releasing efficiency of the hydrogels was analyzed using disc diffusion method. To prepare antibiotic incorporated scaffolds 10 mm discs were prepared and 5, 10, 20 μg respectively of amikacin and vancomycin were loaded by diffusion. Both gram-positive (*Staphylococcus sps.*) and gram-negative bacteria (*Pseudomonas sps.*) used for the study were kindly donated by Polyclinic, Kerala, India. The bacteria were cultured on Muller Hinton agar plates, the antibiotic incorporated scaffolds were placed, incubated at **37^{0}C** for 24 hours and the zone of inhibition was measured. Untreated

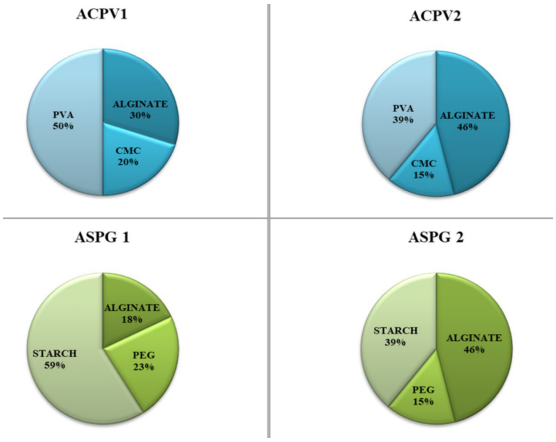

Figure 1: Percentage composition of constituent polymers in ACPV and ASPG hybrid hydrogel subsets

discs were used as control.

Statistical analysis

The results were expressed as mean ± SEM and the statistical analysis for biodegradation studies was performed by Tukey's multiple comparison test. One-sample t test was utilized for protein adsorption studies and morphometry. The level of significance was set at $P<0.05$ for all experiments.

Results

Synthesis of hybrid hydrogels

ACPV hybrid hydrogel system was prepared by interpenetrating alginate and cellulose with the synthetic polymer PVA. ACPV1 and ACPV2 were prepared by varying the ratio of polymer constituents. The natural polymers used in ASPG system included alginate and starch along with the synthetic polymer PEG. The two subsets ASPG1 and ASPG2 were prepared by altering the constituent ratio. Divalent cation, Ca^{2+} was used as the crosslinking agent in all preparations. The percentage composition of alginate, cellulose and PVA were 30%, 20% and 50% respectively for ACPV1 and 46%, 15% and 39% respectively for ACPV2. ASPG1 system contained 17%, 23% and 58% of alginate, PEG, and starch respectively whereas ASPG2 contained 46%, 15% and 39% with respect to alginate, PEG, and starch (**figure 1**).

Surface functional groups

ATR spectra demonstrated similar peaks suggesting the existence of similar functional groups on hydrogel surface (**figures 2A-2D**). The broad peak around 3500cm^{-1} in all the four hydrogels represented -OH stretching vibrations contained in alginate, starch, CMC, PVA and PEG. The sharp peak 1700cm^{-1} attributed to the stretching vibrations of carbonyl groups contained in the alginate. The sharp peak around 1750 cm^{-1} representing stretching vibrations of -COOH is due to the presence of alginate and CMC. Previous analysis of IR spectra of alginate as well as CMC has revealed this

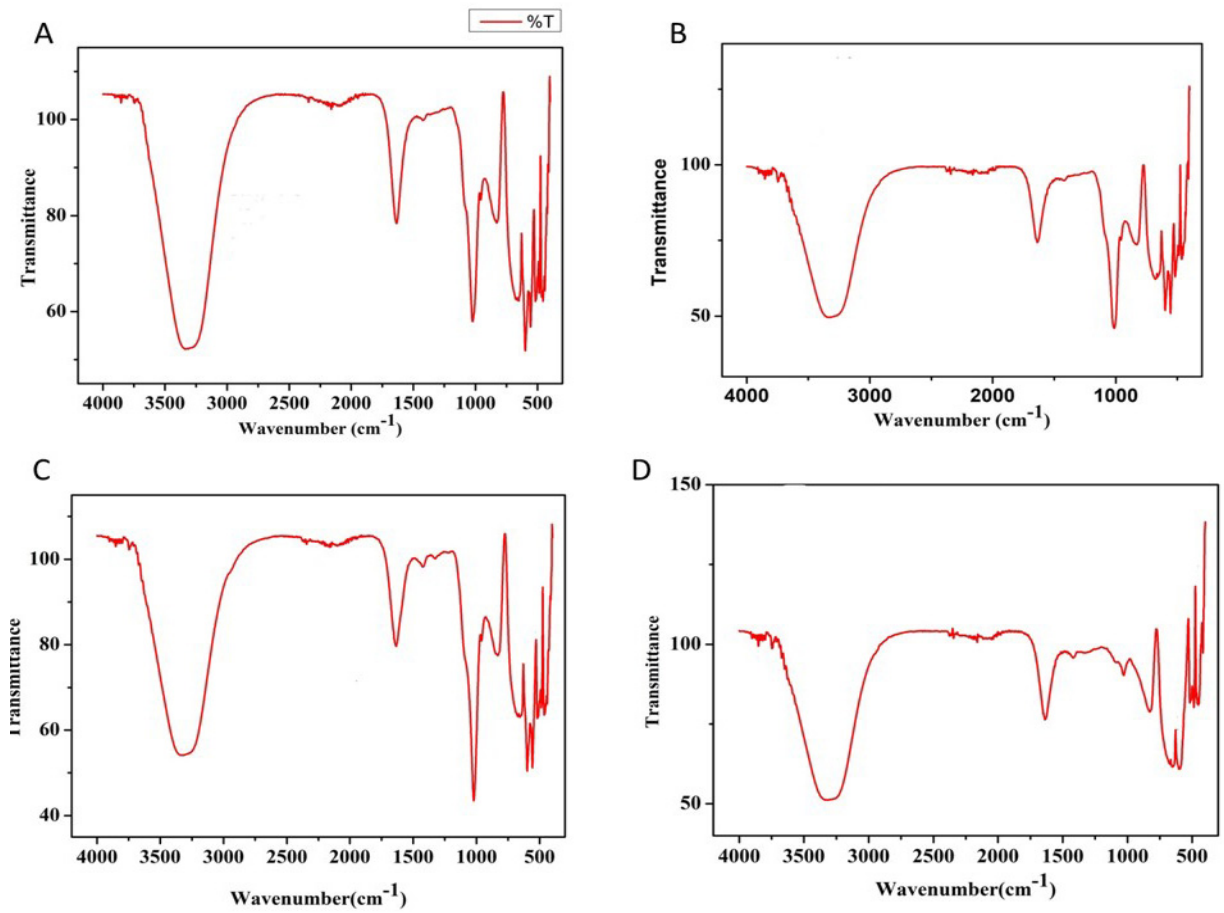

Figure 2: ATR spectra of hybrid hydrogels showing the peaks corresponding to characteristic functional groups: (A) ACPV1, (B) ACPV2, (C) ASPG1 and (D) ASPG2

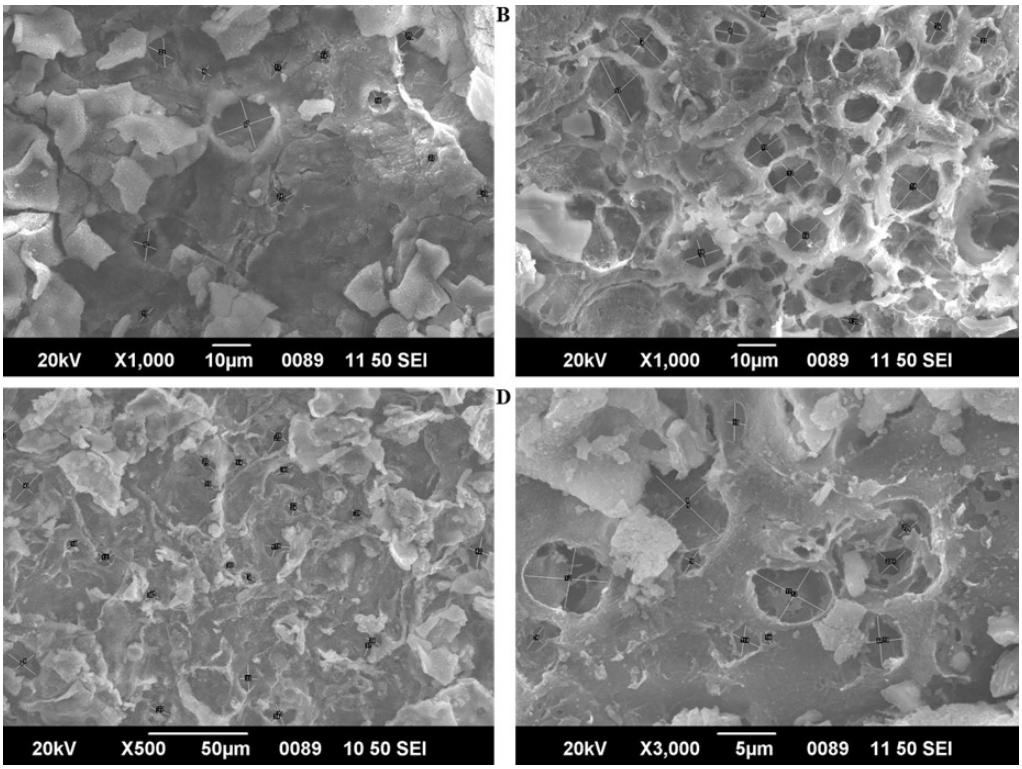

Figure 3: SEM images showing the pore distribution and size of hybrid hydrogel scaffolds: (A) ACPV1, (B) ACPV2, (C) ASPG1 and (D) ASPG2

peak around 1500 cm^{-1}. The sharp peak around 1000 cm^{-1} was due to the C-O-C stretching vibrations which represents the glycosidic bonds in the polysaccharides and in the PVA. Hence, the IR analysis suggests the presence of alginate, starch, CMC, PVA and PEG fractions in the surface of respective hydrogels.

Surface morphology

SEM imaging demonstrated the surface morphology and pore distribution of the hydrogels unveiling the porous morphology, pore density and pore interconnectivity (**figures 3A-3D**). ACPV2 and ASPG1 exhibited increased pore diameter when compared to ACPV1 and ASPG2 (**table 1**). However, there difference in pore length and breadth between ACPV1 (P=0.0753) and ACPV2 (P=0.1089), ACPV1 (P=0.3158) and ASPG2 (P=0.1348) and ACPV2 (P=0.7082) and ASPG 1 (P=0.9839) were statistically not significant. Interestingly, the pore length and breadth in ACPV1 (P=0.0017) and ASPG1 (P=0.0229), ACPV2 (P=0.0007) and ASPG2 (P=0.0002), and ASPG1 (P<0.0001) and ASPG2 (P<0.0001) were statistically significant. Additionally, the pore aspect ratio of the hydrogels exhibited similar values and were statistically not significant suggesting the similar pore morphology (**table 1**).

Water profile

The EWC and water holding capacity of hybrid hydrogels displayed EWC >79% and swelling ratio >5; however, were statistically not significant among the groups except for the EWC between ASPG2

Table 1: Characterization of ACPV and ASPG hydrogels

Parameters	ACPV 1	ACPV2	ASPG1	ASPG2
Equilibrium water content	82.44 ± 4.58	88.40 ± 2.51	83.50 ± 5.09	78.57 ± 10.37
Swelling	6.00 ± 1.76	8.94 ± 2.21	6.43 ± 1.77	5.33 ± 2.08
Pore length	6.67 ± 3.31	10.35 ± 3.60	11.76 ± 4.20	4.03 ± 2.41
Pore breadth	5.20 ± 2.90	7.63 ± 2.70	7.96 ± 2.50	2.84 ± 1.72
Pore aspect ratio	1.34 ± 0.31	1.36 ± 0.20	1.48 ± 0.35	1.41 ± 0.29
Receding contact angle	44.44 ± 5.21	52.46 ± 4.40	45.14 ± 3.58	46.09 ± 7.94
Advancing contact angle	43.33 ± 4.51	48.88 ± 4.40	45.15 ± 4.8	47.2 ± 7.98
Tensile Strength	0.38 ± 0.06	0.47 ± 0.13	0.15 ± 0.07	0.91 ± 0.003
Young's Modulus	0.98 ± 0.15	1.51 ± 0.36	1.66 ± 0.37	4.50 ± 0.02
Protein adsorption (%)	41.05 ± 31.24	41.40 ± 19.60	75.42 ± 14.88	46.73 ± 26.83

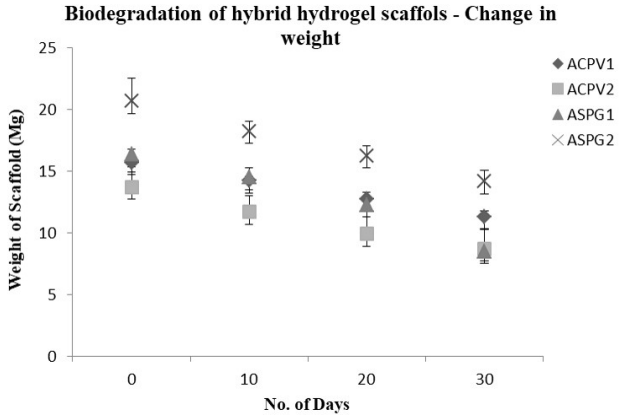

Figure 4: Biodegradation of hydrogels showing the progressive loss in dry weight

and ACPV2 (P=0.0207) (**table 1**). Interestingly, ACPV2 exhibited increased level of EWC (88.40±2.51) suggesting the super absorbent nature. Overall, the four hydrogels exhibited similar water profile (**table 1**).

Tensile Strength

ASPG2 exhibited significantly greater tensile properties when compared with other three hydrogels. The tensile strength of ACPV1 (P=0.7138) was higher than ASPG1 and lower than ACPV2 (P=0.1213 respectively); however, the difference was statistically not significant. ASPG2 exhibited increased Young's modulus compared to the other three hydrogels; however, the increase was statistically not significant (**table 1**).

Table 2: Biodegradation of ACPV and ASPG hydrogels showing the alterations in TDS and pH

Hydrogel	TDS	PH
	DAY 1	
ACPV1	3582 ± 0	7.10 ± 0
ACPV2	3582 ± 0	7.10 ± 0
ASPG1	3582 ± 0	7.10 ± 0
ASPG2	3582 ± 0	7.10 ± 0
	DAY 10	
ACPV1	4609 ± 257	6.90 ± 0.03
ACPV2	4453 ± 198	6.90 ± 0.10
ASPG1	4343 ± 40	6.80 ± 0.05
ASPG2	4137 ± 1723	6.75 ± 0.07
	DAY 20	
ACPV1	5010 ± 428	6.80 ± 0.015
ACPV2	5213 ± 328	6.85 ± 0.02
ASPG1	5429 ± 46	6.75 ± 0.05
ASPG2	5399 ± 519	6.80 ± 0.005
	DAY 30	
ACPV1	5864 ± 596	7.08 ± 0.06
ACPV2	5691 ± 361	7.13 ± 0.02
ASPG1	6041 ± 462	7.03 ± 0.15
ASPG2	6006 ± 540	7.10 ± 0

Surface hydrophilicity

The advancing contact angles (ACA) of the hydrogels ranged between 43° to 48° whereas the receding contact angles (RCA) were between 44° and 52° suggesting the amphiphilic nature of the hydrogels; however, difference between ACA or RCA among the hydrogels were statistically not significant (**table 1**).

Biodegradation

Weight loss in ASPG1 hydrogel was minimal till day 10 when compared to the initial dry weight (P>0.05) followed by significant increase in weight loss as observed in days 20 and 30. A significant weight loss was shown by ASPG2 hydrogels in days 10 and 20; however, the weight loss after 20 days was statistically not significant (p>0.05) . Additionally, the trend for weight loss was similar for ACPV hydrogels as minimal weight loss was observed in both hydrogels till day 10 and was significantly increased in day 30 for both hydrogels (p<0.05) (**figure 4**). TDS showed gradual increase throughout the course of the experiment which was significantly higher in day 30 when compared with day 1 (p<0.05) for all the hydrogels (**table 2**). The pH was slightly acidic during the initial phase and turned to neutral or slightly alkaline on day 30. The initial and final pH of the medium was statistically insignificant (p>0.05). However, the variations were significant on day 10 and 20 when compared with day 1 for all the scaffolds (p<0.05) (**table 2**).

Protein adsorption

The total proteins adsorbed on hydrogel surfaces were 41.05%, 49.4%, 75.4% and 46.7% for ACPV1, ACPV2, ASPG1 and ASPG2 respectively (**table 1**). The level of protein adsorption was significantly higher (P=0.0466) ASPG1 hydrogel; however, was statistically not significant in ACPV1, ACPV2 and ASPG2 (P=0.2283, P=0.1036 and P=0.0752 respectively). SDS PAGE analysis revealed predominant albumin adsorption onto the surface of all hydrogels. The relative albumin adsorption was 60.33%, 53.75%, 50.17%, and 56.25% respectively for ACPV1, ACPV2, ASPG1 and ASPG2 where plasma control presented 80.47% (**figure 5**).

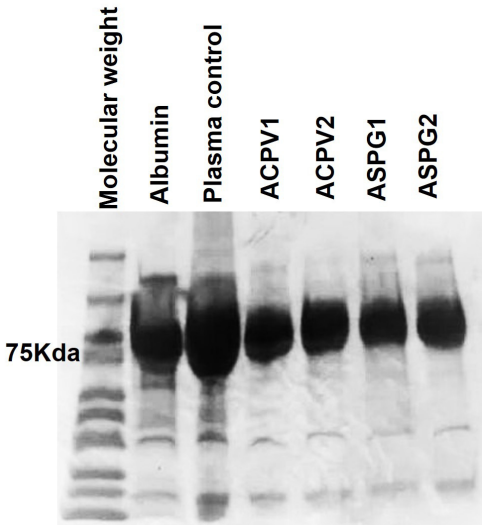

Figure 5: SDS-PAGE analysis of hybrid hydrogels after treatment with plasma demonstrating the conspicuous band corresponding to adsorption of albumin in comparison with control plasma and bovine serum albumin

Cytocompatibility

The H9c2 cells on contact with all the hydrogels retained their normal spindle morphology and deviation from the normal morphology was completely absent suggesting the non-toxic nature of the hydrogels revealing their biocompatibility (**figure 6A-6E**). MTT assay using H9c2 cells cultured with hydrogel extract revealed the viability 82%, 105.37%, 89.12% and 104.75% for ACPV1, ACPV2, ASPG1 and ASPG2 respectively when compared with the control (**figure 6F**). The difference in viability was statistically not significant among the groups ($p>0.05$) .

Antimicrobial Efficiency

ACPV and ASPG hydrogel subsets incorporated with different concentrations of amikacin and vancomycin exhibited significant increase in zone of inhibition when compared with the control (**table 3, figure 7**). Statistically significant increase in the zone of inhibition was observed between ACPV1(5_{Ami}) and ASPG1(5_{Ami}). However, the variations in zone of inhibition were statistically not significant for the other hydrogels incorporated with 5, 10 and 20µl of amikacin ($p>0.05$). In addition, ACPV1(5_{Vanc}) showed significant difference ($p<0.05$) between ACPV2(5_{Vanc}) and ASPG1(5_{Vanc}); however, was statistically not significant compared to ACPV1(5_{Vanc}) and ASPG2(5_{Vanc}) ($p>0.05$). Similarly, ACPV2(5_{Vanc}) exhibited significant increase than ASPG1(5_{Vanc}) and ASPG2(5_{Vanc}) ($p<0.05$) ; however, ASPG1(5_{Vanc}) and ASPG2(5_{Vanc}) displayed similar trend. ACPV1(10_{Vanc}) and ACPV2(10_{Vanc}) exhibited significant increase in zone of inhibition when compared with ASPG1(10_{Vanc}) and ASPG2(10_{Vanc}) ($p<0.05$); however, the zone of inhibition among ACPV1(10_{Vanc}) and ACPV2(10_{Vanc}) and ASPG1(10_{Vanc}) and ASPG2(10_{Vanc}) were statistically not significant ($p>0.05$). Also, non-significant variation was observed for any of the hydrogels incorporated with 20µl of vancomycin ($p>0.05$).

Discussions

The panel of hydrogel scaffolds synthesized in this study were decorated with ample functional moieties contributing to the biological performance for cardiac applications. Evidently, IR analysis revealed the presence of abundant hydrophilic functional groups such as hydroxyl, carboxyl, and carbonyl on scaffold surface. The sharp peak near 1000 cm^{-1} which indicated C-O-C stretching in all hydrogels confirms the presence of polysaccharides as this vibration is characteristic for the glycosidic bonds in polysaccharides. Also, the weakening of C-O stretching vibration in ASPG3 reflects increased hydrogen bond formation between glycosidic oxygen and -OH groups indicative of a hydrophilic surface stabilized by hydrogen bonding. Importantly, the presence of hydrophilic moieties on scaffold surface greatly enhances the water absorption capacity of the hydrogels by promoting hydrogen bonding with water molecules [12]. Moreover, the abundance of surface functional moieties provides opportunities for chemical immobilization of biomolecules and other growth factors for improving cell adhesion and maturation [13].

The growth and survival of cells seeded in tissue engineering scaffolds is greatly influenced by its porosity, pore density, and pore size as the cell adhesion, migration, proliferation, differentiation, and cell-cell interaction are dependent on pore architecture [7]. Furthermore, the efficiency of nutrient trafficking and removal of metabolic exhaust is greatly influenced by pore morphology and density. The surface morphometry reveals that the four scaffolds displays pore architecture with pore length ranging between 4 µm to 12 µm and pore breadth ranging between 3 µm to 8 µm corresponding to the micro porous architecture an ideal tissue engineering scaffold [14]. Multiple reports conclude that microporous scaffold architecture improves cell migration,

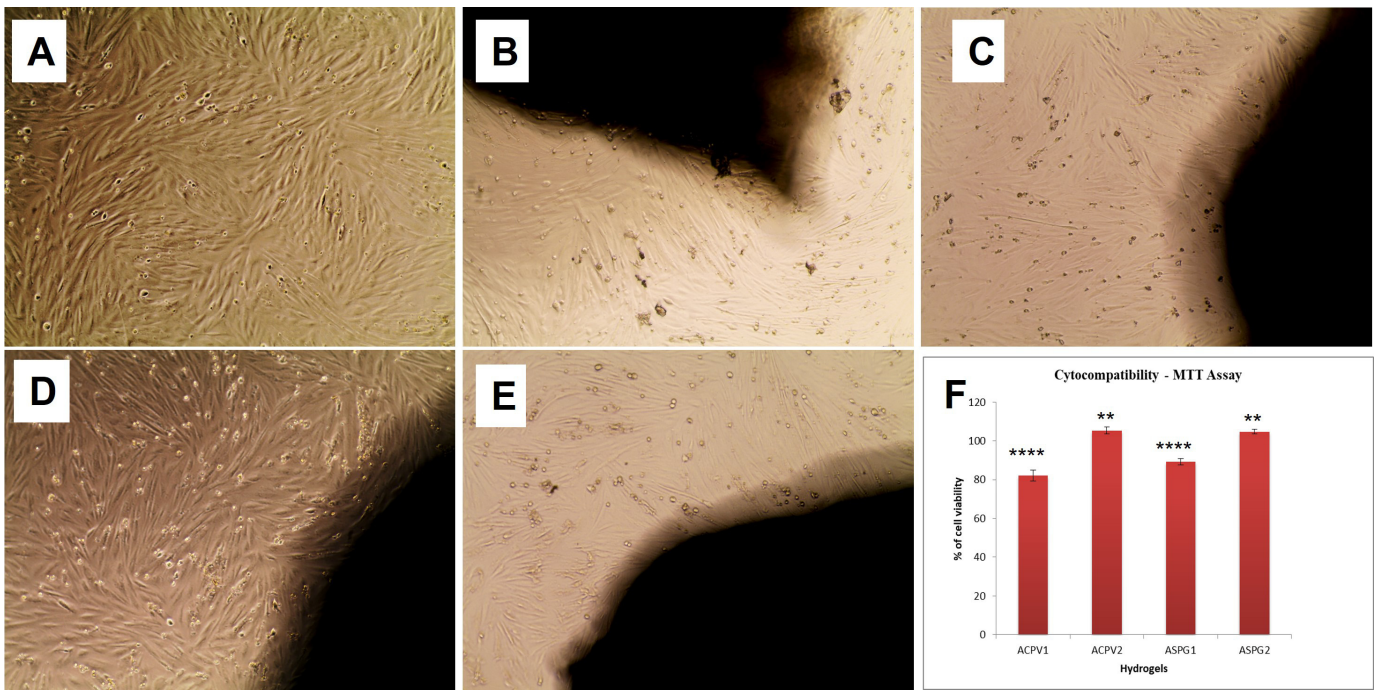

Figure 6: Direct contact assay of hybrid hydrogels using H9c2 cells showing the biocompatibility: (A) Control, (B) ACPV1, (C) ACPV2, (D) ASPG1, and (E) ASPG2. (F) MTT assay using hydrogel extract treated H9c2 cells showing increased cell viability

Table 3: Antimicrobial efficiency of Amikacin and Vancomycin loaded hydrogels revealing the zone of inhibition

Hydrogel	Amikacin			Vancomycin		
	5 µg/mL	10 µg/mL	20 µg/mL	5 µg/mL	10 µg/mL	20 µg/mL
ACPV1	2.37 ± 0.05	2.47 ± 0.05	2.73 ± 0.11	2.53 ± 0.11	3.03 ± 0.05	3.16 ± 0.05
ACPV2	2.30 ± 0.10	2.53 ± 0.11	2.87 ± 0.05	2.87 ± 0.05	3.20 ± 0.20	3.06 ± 0.05
ASPG1	2.06 ± 0.05	2.53 ± 0.05	2.66 ± 0.05	2.20 ± 0.10	2.63 ± 0.05	2.96 ± 0.15
ASPG2	2.23 ± 0.11	2.47 ± 0.11	2.76 ± 0.05	2.30 ± 0.20	2.63 ± 0.11	3.06 ± 0.05

attachment, and anchorage dependent cell to cell communication [15]. Moreover, neovascularization, fibroblast infiltration and cell survival are optimum in scaffolds with pore size range of 5 µm to 15 µm [16]. Interestingly, human embryonic stem cells (hESCs) demonstrated appreciable attachment on membranes with pore size ranging between 3 to 8 µm [17]. Additionally, poly(ethylene glycol) scaffolds with pore size of 12µm promoted better migration of mesenchymal stem cells (MSCs) [18]. These observations suggest that ASPG and ACPV hydrogels pose immense potential to support the growth of multiple cell types onto the interstices.

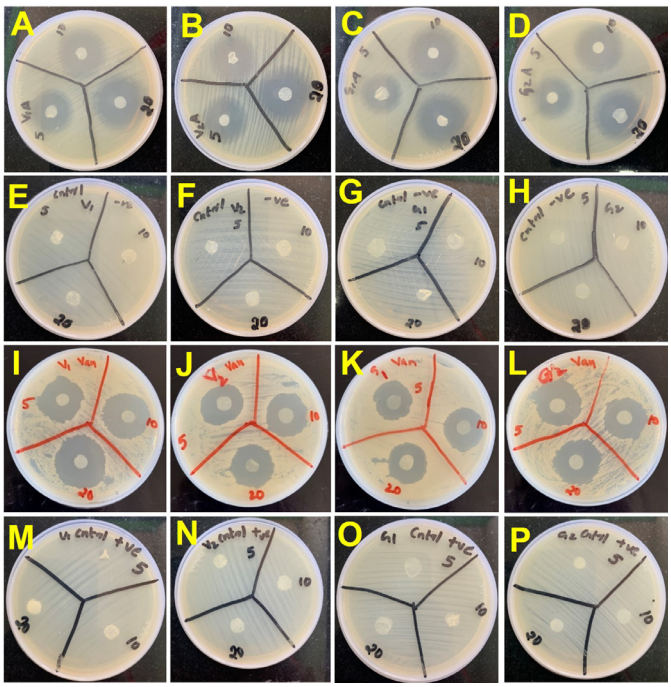

Figure 7: Antibiotic releasing efficiency of ACPV and ASPG hybrid hydrogel scaffolds (A) ASPV1incorporatred with different concentrations of amikacin (B) ACPV2 incorporated with different concentrations of amikacin (C) ASPG1 incorporated with different concentrations of amikacin (D) ASPG2 incorporated with different concentrations of amikacin (E) ACPV1 control for amikacin (F) ACPV2 control for amikacin (G) ASPG1 control for amikacin (H) ASPG2 control for amikacin (I) ACPV1 incorporated with different concentrations of vancomycin (J) ACPV2 incorporated with different concentrations of vancomycin (K) ASPG1 incorporated with different concentrations of vancomycin (L) ASPG2 incorporated with different concentrations of vancomycin (M) ACPV1 control for vancomycin (N) ACPV2 control for vancomycin (O) ASPG1 control for vancomycin (P) ASPG2 control for vancomycin.

Water content of the hydrogels is the function of osmotic driving forces and the cohesive force exerted by the polymer network [19]. Both ACPV and ASPG hydrogel subsets demonstrated an EWC greater than 80% and swelling ratio between 5-7 attributing to ample hydrophilic functional groups and porosity as evidenced by IR analysis and SEM respectively. The superior water content is beneficial for in trafficking of metabolite and mass transfer. In addition, the increased water level relaxes the polymer chains to increase the surface area and pore size facilitating the cell survival and performance. [20]. Furthermore, the increased water content prevents dehydration thereby accelerating the wound healing responses [21]. Hence, the superior water content in the hydrogels favour for successful CTE.

Biodegradation of hybrid hydrogels were studied using PBS buffer for 30 days where all the hydrogels maintained their structure for the initial three weeks period followed by slower withering. ACPVI and ACPV2 hydrogels lost 72% and 63.5% of their dry weight respectively after 30 days study. Similarly, ASPG1 and ASPG 2 hydrogels lost 52% and 81.6% of their dry weight respectively. TDS were increased in a time dependent fashion owing to the erosion of ions and other solid particles from the hydrogel surfaces confirming the degradation. Crosslinking of the polymer chain with calcium is affected by the formation of covalent bond between calcium ions and guluronic acid residues in the G block of alginate chains forming the characteristic egg box structure [8]. Interactions of the crosslinked alginate with monovalent ions such as sodium and potassium results in the replacement of calcium ions with monovalent ions result in the collapse of egg box leading to gel-sol transition and subsequent weakening the hydrogel [22]. Additionally, the slight drop in pH suggests the release of mild acidic degradation products which elicits minimal physiological responses owing to the efficient buffering capacity of circulating fluids [8].

Mechanical properties of the CTE scaffolds influence the cell adhesion, cell signalling pathways, angiogenesis, and neo-tissue formation. The superior tensile properties of ACPV2 and ASPG2 hydrogels reflect the increased crosslinking density owing to the increased level of alginate. The Youngs modulus of the hydrogels ranged between 1 to 4 MPa which has been reported to be ideal for soft tissue engineering. For instance, the electrospun polyester ether(urethane urea) scaffold with an elastic modulus ranging between 1-2 MPa was loaded with adeno associated viral genes and implanted into left ventricle of rat resulted in improved LV function owing to the mechanical properties of the scaffold [23] Interestingly, the ACPV and ASPG hydrogels are mechanocompatible for CTE allowing the tuneable mechanical properties by manipulating the crosslinking density by divalent cations.

The contact angle value of all the scaffolds falls within the range of amphiphilicity which is crucial in enhancing cell adhesion and

proliferation [24]. The hydrophilicity of ACPV and ASPG hybrid hydrogel subsets owe to the presence of hydrophilic functional groups such as -COOH, and -OH on hydrogel surfaces as indicated by IR analysis. However, extremely hydrophilic, or hydrophobic surfaces are less favourable for cell adhesion whereas moderately wettable surfaces are optimal for cell adhesion and proliferation [25–27]. Hence, the amphiphilic nature of the hydrogels supports protein adsorption and the attachment, proliferation and migration of cells which is necessary for the integration of CTE implants.

The *in vivo* biocompatibility of a scaffold is greatly driven by the type and amount of protein adsorbed on the surface [28]. Post-implantation, cellular attachment on any scaffold surface is largely affected and regulated by the adsorbed protein layer as scaffold-protein interaction occurs prior to cell infiltration/adhesion. Protein adsorption on a hydrophobic scaffold surface is largely governed by hydrophobic interactions whereas on a hydrophilic surface favour electrostatic force. Interestingly, the hydrophilic surfaces retain confirmation of adsorbed proteins whereas hydrophobic results in structural deformities [29]. The adherence of albumin in the surface of scaffold results in smoothness and a rough surface is detrimental as the RBC membrane rupture occurs upon encountering circulation resulting in haemolysis, and activation and aggregation of platelets leading to thrombosis [30]. Importantly, adsorption of plasma albumin prevents unfavourable cell-scaffold interactions contributing to hemocompatibility and created favourable environment for the infiltrating cells [31]. Additionally, albumin binding on scaffold surface prevents the adsorption of fibrinogen preventing thrombosis and inflammation [32]. Also, there are reports on using albumin itself as biomaterial for fabricating tissue engineering scaffolds due to its exceptional biocompatibility [33]. In the present study, ACPV1, ACPV2 and ASPG2 exhibited superior adsorption of albumin from the serum whereas ASPG1 demonstrated a significantly higher adsorption (75%) which is attributed to the microporous and amphiphilic nature of scaffolds [34].

Importantly, the hydrogels are biocompatible, and the degradation products are non-toxic to the cells. Direct contact revealed the absence of morphological changes in H9c2 cells demonstrating the cytocompatibility of ACPV and ASPG hydrogels. Hence, the ACPV and ASPG hydrogel systems represent biocompatible templates for CTE applications. However, the translational challenges in tissue engineering strategy including infection following the invasive procedures are alarming [35]. Such infections result in unpredictable aftermaths including sustained inflammatory responses leading to treatment failure. Oral/intravenous administration of antibiotics help to prevent infections; however, limited bioavailability and bioretention of antibiotics at the surgery site, and antibiotic resistance are challenging. In addition, the higher doses of antibiotics cause off target side effects including liver damage, and kidney disorders. A possible alternative to treat implant-driven infection is to incorporate antibiotics into scaffolds aiding in a sustained and localized delivery of antibiotics and eliminates the chances of systemic toxicity. In the present study, all the hydrogels incorporated with different concentrations of amikacin and vancomycin demonstrated excellent inhibition of bacterial proliferation. The exceptional hydrophilicity of the ACPV and ASPG enabled the loading/release of antibiotics by simple diffusion. Despite the establishment of the proof of the concept, the efficiency cell performance in antibiotic loaded ACPV and ASPG hydrogels warrants further optimization. However, our approach opens novel translational avenues for the management of nocosominal infections following CTE implantation.

Conclusion

In the present study, two sets of hybrid hydrogel viz ACPVs and ASPGs were prepared for cardiac tissue engineering and evaluated for physical and cytocompatibile properties. The results showed that all the scaffolds were biodegradable with appreciable mechanical strength, optimum surface features, and water holding capacity and evoked no toxicological responses towards seeded cells. All the scaffolds were found to be promising for cardiac tissue engineering.

Acknowledgement: SKC is grateful to the staffs and scholars of KKTMGC and Christ College for their support to complete this study.

Conflict of Interest: All the authors have read the manuscript and declare no conflict of interest. No writing assistance was utilized in the production of this manuscript.

Funding: The authors did not receive any funding for this study.

Availability of data and materials: Data with the raw counts matrices and annotation are available upon request from the authors through proper channels.

References

1. Majid Q.A., Fricker A.T.R., Gregory D.A., et al., Natural Biomaterials for Cardiac Tissue Engineering: A Highly Biocompatible Solution. Front Cardiovasc Med, 7, 554597 (2020).
2. Virani S.S., Alonso A., Aparicio H.J., et al., Heart Disease and Stroke Statistics-2021 Update: A Report from the American Heart Association. Circulation, 143, e254–e743 (2021).
3. Arjmand B., Abedi M., Arabi M., et al., Regenerative Medicine for the Treatment of Ischemic Heart Disease; Status and Future Perspectives. Front Cell Dev Biol, 9, 704903 (2021).
4. Ikada Y. Challenges in tissue engineering, J R Soc Interface 3, 589–601 (2006).
5. Neltner T.G., Kulkarni N.R., Alger H.M., et al., Navigating the U.S. Food Additive Regulatory Program. Compr Rev Food Sci Food Saf 10, 342–368 (2011).
6. Hutmacher D.W., Scaffold design and fabrication technologies for engineering tissues - state of the art and future perspectives. J. Biomater Sci Polym Ed, 12, 107–124 (2001).
7. Finosh G.T., Jayabalan M., Regenerative therapy and tissue engineering for the treatment of end-stage cardiac failure: new developments and challenges. Biomatter, 2, 1–14 (2012).
8. Gnanaprakasam Thankam F., Muthu J., Sankar V., Kozhiparambil Gopal R., Growth and survival of cells in biosynthetic poly vinyl alcohol–alginate IPN hydrogels for cardiac applications. Colloids Surf B Biointerfaces, 107, 137–145 (2013).
9. Gnanaprakasam Thankam F., Muthu J., Alginate based hybrid copolymer hydrogels—influence of pore morphology on cell-material interaction. Carbohydr Polym, 112, 235–244 (2014).
10. Finosh G.T., Jayabalan M., Vandana S., Raghu K.G., Hybrid alginate-polyester bimodal network hydrogel for tissue engineering—Influence of structured water on long-term cellular growth. Colloids Surf B Biointerfaces, 135, 855–864 (2015).
11. Thankam F.G., Diaz C., Chandra I., et al., Hybrid interpenetrating hydrogel network favoring the bidirectional migration of tenocytes for rotator cuff tendon regeneration. J Biomed Mater Res B Appl Biomater, 110, 467–477 (2022).
12. Singh M.R., Patel S., Singh D., Natural polymer-based hydrogels as scaffolds for tissue engineering. In: Nanobiomaterials in Soft Tissue Engineering. Elsevier, pp 231–260 (2016).
13. Niemczyk-Soczynska B., Gradys A., Sajkiewicz P., Hydrophilic Surface Functionalization of Electrospun Nanofibrous Scaffolds in Tissue Engineering. Polymers, 12, 2636 (2020).
14. Vagaská B., Bacáková L., Filová E., Balík K., Osteogenic cells on bio-inspired materials for bone tissue engineering. Physiol Res, 59, 309–322 (2010).
15. Bru•auskait I., Bironait D., Bagdonas E., Bernotien E., Scaffolds and cells for tissue regeneration: different scaffold pore sizes-different cell effects. Cytotechnology, 68, 355–369 (2016).
16. Thankam F.G., Muthu J., Influence of physical and mechanical properties

of amphiphilic biosynthetic hydrogels on long-term cell viability. J Mech Behav Biomed Mater, 35, 111–122 (2014).
17. Kim S., Ahn S.E., Lee J.H., et al., A novel culture technique for human embryonic stem cells using porous membranes. Stem Cells Dayt Ohio, 25, 2601–2609 (2014).
18. Peyton S.R., Kalcioglu Z.I., Cohen J.C., et al., Marrow-Derived stem cell motility in 3D synthetic scaffold is governed by geometry along with adhesivity and stiffness. Biotechnol Bioeng, 108, 1181–1193 (2011).
19. El-Sherbiny I.M., Yacoub M.H., Hydrogel scaffolds for tissue engineering: Progress and challenges. Glob Cardiol Sci Pract, 2013, 316–342 (2013).
20. Coenen A.M.J., Bernaerts K.V., Harings J.A.W., et al., Elastic materials for tissue engineering applications: Natural, synthetic, and hybrid polymers. Acta Biomater, 79, 60–82 (2018).
21. Saravanan S., Chawla A., Vairamani M., et al., Scaffolds containing chitosan, gelatin and graphene oxide for bone tissue regeneration in vitro and in vivo. Int J Biol Macromol, 104, 1975–1985 (2017).
22. Kurowiak J., Kaczmarek-Pawelska A., Mackiewicz A.G., Bedzinski R., Analysis of the Degradation Process of Alginate-Based Hydrogels in Artificial Urine for Use as a Bioresorbable Material in the Treatment of Urethral Injuries. Processes, 8, 304 (2020).
23. Gu X., Matsumura Y., Tang Y., et al., Sustained viral gene delivery from a micro-fibrous, elastomeric cardiac patch to the ischemic rat heart. Biomaterials, 133, 132–143 (2017).
24. Ghorbani F., Sahranavard M., Mousavi Nejad Z., et al., Surface Functionalization of Three Dimensional-Printed Polycaprolactone-Bioactive Glass Scaffolds by Grafting GelMA Under UV Irradiation. Front Mater, 7, 528590 (2020).
25. Lin G., Zhang X., Kumar S.R., Mark J.E., Improved Hydrophilicity from Poly(ethylene glycol) in Amphiphilic Conetworks with Poly(dimethylsiloxane). Silicon, 1, 173–181 (2009).
26. van Wachem P.B., Hogt A.H., Beugeling T., et al., Adhesion of cultured human endothelial cells onto methacrylate polymers with varying surface wettability and charge. Biomaterials 8, 323–328 (1987).
27. van Wachem P.B., Beugeling T., Feijen J., et al., Interaction of cultured human endothelial cells with polymeric surfaces of different wettabilities. Biomaterials, 6, 403–408 (1985).
28. Yu Q., Chen H., Interaction of switchable biomaterials surfaces with proteins. In, Switchable and Responsive Surfaces and Materials for Biomedical Applications. Elsevier, pp 167–188 (2015).
29. Recek N., Mozetic M., Jaganjac M., et al., Adsorption of Proteins and Cell Adhesion to Plasma Treated Polymer Substrates. Int J Polym Mater Polym Biomater, 63, 685–691 (2014).
30. Maruyama O., Nishida M., Yamane T., et al., Hemolysis resulting from surface roughness under shear flow conditions using a rotational shear stressor. Artif Organs, 30, 365–370 (2006).
31. Gnanaprakasam Thankam F., Muthu J., Influence of plasma protein–hydrogel interaction moderated by absorption of water on long-term cell viability in amphiphilic biosynthetic hydrogels. RSC Adv, 3, 24509 (2013).
32. Radhakrishnan A.., Jose G.M., Kurup M., PEG-penetrated chitosan–alginate co-polysaccharide-based partially and fully cross-linked hydrogels as ECM mimic for tissue engineering applications. Prog Biomater, 4, 101–112 (2015).
33. Li P.S. Liang Lee I., Yu W.L. et al., A Novel Albumin-Based Tissue Scaffold for Autogenic Tissue Engineering Applications. Sci Rep 4, 5600 (2015).
34. Zhang K., Fan Y., Dunne N., Li X., Effect of microporosity on scaffolds for bone tissue engineering. Regen Biomater 5, 115–124 (2018).
35. Kandi V., Vadakedath S., Implant-Associated Infections: A Review of the Safety of Cardiac Implants. Cureus 12, e12267 (2020).